Motor Cost Re-Optimization in Indirect Human Movement Pattern Adaptation

Yangmengfei Xu * **Vincent Crocher** * **Justin Fong** * **Ying Tan** * **Denny Oetomo** *

* *Human Robotics Lab, Department of Mechanical Engineering, The University of Melbourne, Melbourne, Australia, (e-mail: {yangmengfei,vcrocher,fong.j,yingt,doetomo}@unimelb.edu.au).*

Abstract: Human movement resolves kinematic redundancy by organizing high-dimensional joint activity into low-dimensional coordination patterns, or synergies, which are plastic and can be reshaped for rehabilitation and skill training. While explicit error correction can reduce task errors, it may also induce slacking, limiting genuine learning. Indirect Shaping Control (ISC) was proposed to induce movement pattern change implicitly, without explicit reference trajectories. In a previous experiment, 20 participants performed reaching tasks while a robotic system applied a hand force that varied with the arm's swivel angle, creating an energetic bias that altered their movement patterns. Although this setup induced adaptation under ISC, the underlying motor-cost mechanisms remained unquantified. In this work, we retrospectively analyzed the same dataset using a rigid-body inverse-dynamics model to estimate motor cost associated with swivel-angle change. Motor cost was quantified using the Torque-Time Integral (TTI) and decomposed into natural and robot-induced components, linking cost variation to swivel angle and hand velocity. This study provides a quantitative description of implicit adaptation and insights for designing effective implicit interventions.

Keywords: Human Movement Pattern Adaptation, Motor Control, Rehabilitation Robotics

1. INTRODUCTION

Human movement is intrinsically redundant: the musculoskeletal system has more degrees of freedom (DOFs) than necessary to execute most tasks. To resolve this redundancy, the central nervous system (CNS) organizes motor output into low-dimensional coordination patterns, or synergies (McMorland et al., 2015). Importantly, these synergies are plastic and reorganize under novel dynamics, suggesting that movement patterns can be reshaped. For instance, pathological synergies in stroke may represent local minima in a damaged motor cost landscape; altering this landscape could drive the CNS to re-optimize toward functionally superior patterns (Levin et al., 2009).

Motor adaptation is commonly modeled as a trade-off between task performance (error minimization) and physiological effort (cost minimization) (Todorov and Jordan, 2002; Emken et al., 2007). Although explicit error correction can reduce movement errors, it may also induce slacking and thereby limit genuine learning (Reinkensmeyer et al., 2009). To leverage CNS plasticity while avoiding slacking, we developed Indirect Shaping Control (ISC), a robotic paradigm that implicitly reshapes movement by acting on the effort component ("motor cost") without explicit error correction (Fong et al., 2019; Xu et al., 2021). Here, "motor cost" refers to the aggregate physical burden required to execute a movement. This cost can be described across multiple dynamic levels, including metabolic energy expenditure, mechanical work or joint torque changes (mechanical dynamics), and neural effort associated with muscle activation (neurological dynamics). In (Xu et al., 2021), 20 participants performed reaching tasks without reference trajectories, while a viscous force field at the hand varied with the arm's swivel angle—the rotation of the elbow around the line from shoulder to hand, which does not affect hand position. This setup created an energy landscape that favored certain movement solutions, and participants adapted their motor output in response to ISC. Although adaptation was observed, the underlying motor-cost mechanisms were not quantitatively modeled, leaving open questions about how natural and induced costs jointly shape behavior.

Understanding these mechanisms requires a quantitative framework for motor costs. Although humans clearly optimize movement, the specific physiological cost function guiding adaptation remains unclear. Kinematic models, such as minimum jerk, predict smooth trajectories but neglect energetic demands (Flash and Hogan, 1985). Dynamic models account for mechanical costs such as joint torque changes or work (Uno et al., 1989; Kang et al., 2005), whereas neurological models incorporate signal-dependent noise to explain movement precision (Todorov and Jordan, 2002). Together, these frameworks indicate that both energetic and neural factors contribute to motor planning, motivating experiments that quantify and manipulate motor costs in interventions such as ISC.

While our previous work (Xu et al., 2021) introduced the ISC paradigm and illustrated the resulting energetic gradient using a theoretical cost simulation, that model relied on a hypothetical grid of speeds and angles and remained conceptual. It did not quantify the physiological costs actually incurred by participants. To address this gap, the current study conducts a retrospective empirical analysis of the dataset by applying a full 4-DOF spatial rigid-body inverse dynamics model (three shoulder DOFs and one elbow DOF) to the recorded kinematic trajectories, thereby resolving the full 3D kinetics associated with changes in swivel angle.

Motor cost is quantified using the Torque-Time Integral (TTI) (Rozand et al., 2015; Russ et al., 2002), which reflects cumulative metabolic demand and is decomposed into natural components (inherent limb dynamics) and artificial components (robotic viscosity). Relating these cost components to changes in swivel angle and hand velocity provides a quantitative description of implicit adaptation and insight into how altering the weighting of artificial and natural costs can guide motor adaptation. This study therefore contributes a quantitative decomposition of motor costs during ISC, identifies behavioral strategies that minimize total cost, and provides design insights for implicit interventions aimed at more effectively reshaping movement patterns.

2. EXPERIMENTAL DATA AND SETUP

This study performs a retrospective energetic analysis on a dataset previously described in (Xu et al., 2021). The dataset includes 3D kinematic and kinetic recordings from 20 healthy participants (age 23.9±3.0 years) who provided informed consent (Ethics ID #1749444).

Participants performed repeated reaching movements while holding the handle of the EMU rehabilitative manipulandum (Fong et al., 2017), shown in Figure 1. The EMU is an end-effector robot that allows 3D hand motion; however, due to its passive wrist joint, it does not apply direct torque to the elbow or shoulder, leaving the arm's null-space configuration, represented by the swivel angle θ, unconstrained. Arm kinematics were recorded at 20 Hz using TrakSTAR magnetic sensors at the shoulder, elbow, and wrist, and θ was computed as the angle between the arm plane defined by these landmarks and the vertical plane (Kang et al., 2005), as illustrated in Figure 2(a).

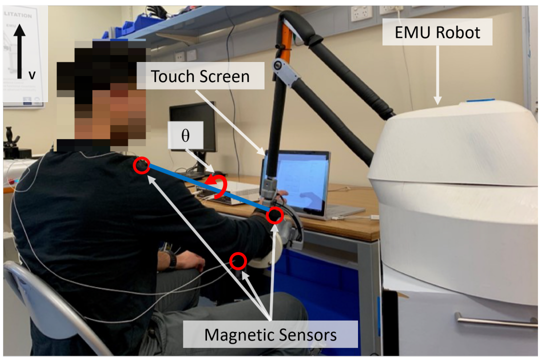

Fig. 1. The experimental setup with the EMU manipulandum, the location of the three magnetic sensors, and the swivel angle representation (θ), where $\mathbf{v}$ is an absolute vertical unit vector.

During the intervention phase, a viscous force field $\mathbf{f}_{vis}$ was applied at the hand to introduce an artificial energetic

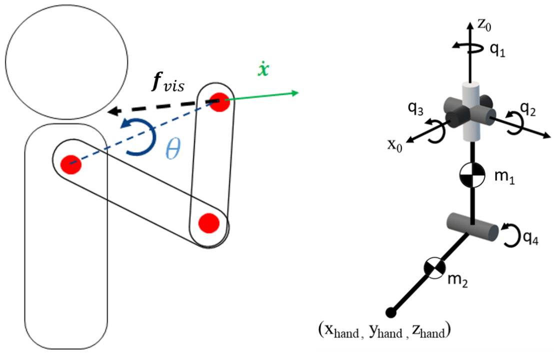

(a) (b)

Fig. 2. (a) The swivel angle representation (θ), hand velocity ($\dot{\mathbf{x}}$), and corresponding viscous force field ($\mathbf{f}_{vis}$). (b) The arm model for cost estimation with four revolute joints and two masses centered on the two links.

cost. The field was modulated by swivel angle θ and hand velocity $\dot{\mathbf{x}}$:

$$\mathbf{f}_{vis} = \begin{cases} -b_i \cdot b_k \cdot (\theta_d - \theta) \cdot \dot{\mathbf{x}} & , \text{ if } \theta_d > \theta \\ 0 & , \text{ otherwise,} \end{cases} \quad (1)$$

where b_k is a constant gain, b_i scales the gradual introduction of the field, and θ_d is the subject-specific target swivel-angle trajectory. This formulation created an energetic gradient in which movements with larger swivel angles, closer to θ_d, encountered less resistance. In the present study, the recorded force profiles were used to estimate the artificial component of motor cost.

Participants completed 200 reaching movements distributed across five phases: FREE, PRE, INT, POST, and AFTER. Briefly, PRE and POST were performed with the robot in transparent mode, INT was performed with the ISC force field active, and FREE and AFTER were performed without the robot attached. Full protocol details are provided in (Xu et al., 2021). Participants were randomly assigned to one of two intervention groups ($N = 10$ per group): Constant-ISC (CG), in which the shaping goal remained fixed at 10°, and Progressive-ISC (PG), in which the shaping goal increased linearly from 0° to 10° before remaining constant.

For the present analysis, we focused on the steady-state portion of the intervention, namely trials 101–135 of the full protocol (INT trials 51–85). In this interval, both groups were exposed to the same robotic condition, with a fixed 10° shaping offset, allowing direct comparison of the energetic strategies adopted under Constant and Progressive shaping. This window also excludes the last 15 trials of the INT phase, during which the force-field intensity was progressively removed through the scaling factor b_i. The desired swivel angle θ_d also increased gradually along the trajectory within each reach, from $\theta_d(d = 0) = 0°$ at movement onset to $\theta_d(d_{\max}) = 10°$ at the end of the reach.

All kinematic data were processed offline for cost estimation. Position signals were low-pass filtered, and velocities and accelerations were obtained by numerical differentiation. For inverse dynamics, the arm was modeled as a two-link rigid body. Segment lengths were measured for each participant, and segment masses were estimated from body mass using standard anthropometric tables (Plagenhoef et al., 1983). These subject-specific anthropometric and kinematic parameters were then used in the TTI-based cost estimation described in Section 3.

3. COST ANALYSIS

3.1 Arm Kinematics Model

To analyze motor cost, the human arm was modeled as a simplified two-link mechanism with a ball joint at the shoulder (modeled as three orthogonal revolute joints) and a single revolute joint at the elbow. The two links represent the upper arm and forearm, with lengths l_1 and l_2, and point masses m_1 and m_2, respectively, as shown in Figure 2(b). This reduced-order model captures the main degrees of freedom relevant to reaching and provides a sufficient basis for inverse dynamics and cost estimation.

The four joint angles are denoted by q_1, q_2, q_3, and q_4, where q_1 represents shoulder internal/external rotation, q_2 shoulder flexion/extension, q_3 shoulder abduction/adduction, and q_4 elbow flexion/extension. The forward kinematics from joint space to task space are:

$$\begin{aligned} x_{hand} &= -\,l_2 c_1 c_2 s_4 - (l_1 + l_2 c_4)(s_1 s_3 + c_1 s_2 c_3), \\ y_{hand} &= -\,l_2 s_1 c_2 s_4 - (l_1 + l_2 c_4)(s_1 s_2 c_3 - c_1 s_3), \\ z_{hand} &= l_2 s_2 s_4 - (l_1 + l_2 c_4) c_2 c_3, \end{aligned} \tag{2}$$

where $c_i = \cos(q_i)$ and $s_i = \sin(q_i)$.

For a given hand position $(x_{\text{hand}}, y_{\text{hand}}, z_{\text{hand}})$, infinitely many joint configurations $\mathbf{q}_n = [q_1\ \ q_2\ \ q_3\ \ q_4]^{\mathrm{T}} \in \mathbb{R}^4$ satisfy the forward kinematics, reflecting arm redundancy. This redundancy can be parameterized by the swivel angle θ:

$$\theta = \arcsin\left(\cos q_1 \cos q_3 + \sin q_1 \sin q_2 \sin q_3\right). \tag{3}$$

Thus, for a given hand position $(x_{\text{hand}}, y_{\text{hand}}, z_{\text{hand}})$ and swivel angle θ, the joint configuration

$$\mathbf{q}_n = [q_1\ \ q_2\ \ q_3\ \ q_4]^{\mathrm{T}} \in \mathbb{R}^4$$

is uniquely determined. This constraint allows the measured task-space trajectories to be mapped into joint space for torque estimation.

3.2 Arm Dynamics Model and Cost Estimation

Motor cost, representing energy expenditure, was estimated using the Torque-Time Integral (TTI) (Russ et al., 2002). TTI was chosen because it captures the isometric metabolic cost of counteracting the viscous force field over time. As subject-specific muscle physiology data were unavailable, equal contribution from all joints was assumed to provide a generalized measure of aggregate effort. TTI was used here as a generalized proxy of cumulative load rather than a complete physiological estimate, especially in this velocity-variable task. The analysis separates cost into two components: the *natural cost*, arising from the limb's inherent dynamics, and the *artificial cost*, induced by the robotic force field.

First, the *natural cost* ($\mathcal{L}_n$) represents the baseline effort required to move the arm against inertia and gravity. The natural torque vector, $\boldsymbol{\tau}_{natural}(t)$, is computed using the standard rigid-body equations of motion:

$$\boldsymbol{\tau}_{natural}(t) = \mathbf{M}(\mathbf{q})\ddot{\mathbf{q}} + \mathbf{C}(\mathbf{q}, \dot{\mathbf{q}})\dot{\mathbf{q}} + \mathbf{G}(\mathbf{q}), \tag{4}$$

where $\mathbf{q}, \dot{\mathbf{q}}, \ddot{\mathbf{q}} \in \mathbb{R}^4$ are the joint position, velocity, and acceleration vectors; $\mathbf{M}(\mathbf{q})$ is the inertia matrix; $\mathbf{C}(\mathbf{q}, \dot{\mathbf{q}})\dot{\mathbf{q}}$ represents the Coriolis and centrifugal terms; and $\mathbf{G}(\mathbf{q})$ is the gravitational torque vector. The natural cost was computed as the time integral of the absolute torque magnitudes across the four joints: $\mathcal{L}_n = \int_0^T \sum_{j=1}^4 \left|\boldsymbol{\tau}^{(j)}_{natural}(t)\right| dt$. Because the experimental data are discrete, the integral is approximated by summing the absolute torque magnitudes at each time step and multiplying by the sampling interval ($\Delta t = 0.05$ s).

Second, the robot imposes an *artificial* load. The torque vector generated by this external force field is:

$$\boldsymbol{\tau}_{artificial}(t) = \mathbf{J}_H^T(t) \cdot \mathbf{f}_{vis}(t), \tag{5}$$

where $\mathbf{J}_H(t)$ is the Jacobian at the hand and $\mathbf{f}_{vis}(t)$ is the viscous force applied by the robot. The artificial cost $\mathcal{L}_a$ was computed as $\mathcal{L}_a = \int_0^T \sum_{j=1}^4 |\boldsymbol{\tau}^{(j)}_{artificial}(t)| dt$.

Finally, the *total cost* ($\mathcal{L}_t$) during the intervention phase includes both the natural limb dynamics and the artificial force field. To capture the net effort, the torque vectors are summed before their magnitudes are computed:

$$\mathcal{L}_t = \int_0^T \sum_{j=1}^4 \left|\boldsymbol{\tau}^{(j)}_{natural}(t) + \boldsymbol{\tau}^{(j)}_{artificial}(t)\right| dt. \tag{6}$$

4. OUTCOME METRICS AND REPRESENTATIVE SUBJECT SELECTION

To support the cost analysis, the 20 participants were retrospectively categorized according to their behavioral outcomes, measured by swivel angle adaptation in (Xu et al., 2021). Normality of the adaptation metric, $\Delta\theta(d_{\max})$, was assessed using the Shapiro–Wilk test, and within-group comparisons (PRE vs. INT) were evaluated using Wilcoxon signed-rank tests with a significance threshold of $p < 0.05$. Based on these results, participants were classified into three categories, as shown in Figure 3: CG-NS (non-significant, $N = 1$), the single participant in the CG group who did not show significant adaptation; CG-S (significant, $N = 9$), participants in the CG group who showed significant adaptation; and PG-S (significant, $N = 10$), participants in the PG group, all of whom showed significant adaptation.

To quantify the energetic effect of the robotic intervention, we evaluated the relative cost variation between the trials with the lowest and highest average swivel angle changes, $\Delta\bar{\theta}_{\min}$ and $\Delta\bar{\theta}_{\max}$. Two metrics were defined: the *total cost variation* (ϕ_t) and the *artificial component contribution* (ϕ_a). Both were normalized by the total cost at the baseline configuration, $\mathcal{L}_t(\Delta\bar{\theta}_{\min})$, to express percentage changes relative to the subject's initial load. The total cost variation is

$$\phi_t = \left(\mathcal{L}_t(\Delta\bar{\theta}_{\max}) - \mathcal{L}_t(\Delta\bar{\theta}_{\min})\right) / \mathcal{L}_t(\Delta\bar{\theta}_{\min}) \times 100\%, \tag{7}$$

and the artificial contribution is

$$\phi_a = \left(\mathcal{L}_a(\Delta\bar{\theta}_{\max}) - \mathcal{L}_a(\Delta\bar{\theta}_{\min})\right) / \mathcal{L}_t(\Delta\bar{\theta}_{\min}) \times 100\%. \tag{8}$$

Because both metrics are normalized by the same baseline, the total cost variation can be approximated as $\phi_t \approx \phi_a + \phi_n$, allowing separation of the adaptation associated with the robotic intervention from that associated with natural biomechanical constraints.

To illustrate continuous cost trends, one representative subject was selected from each group (CG-NS, CG-S, and

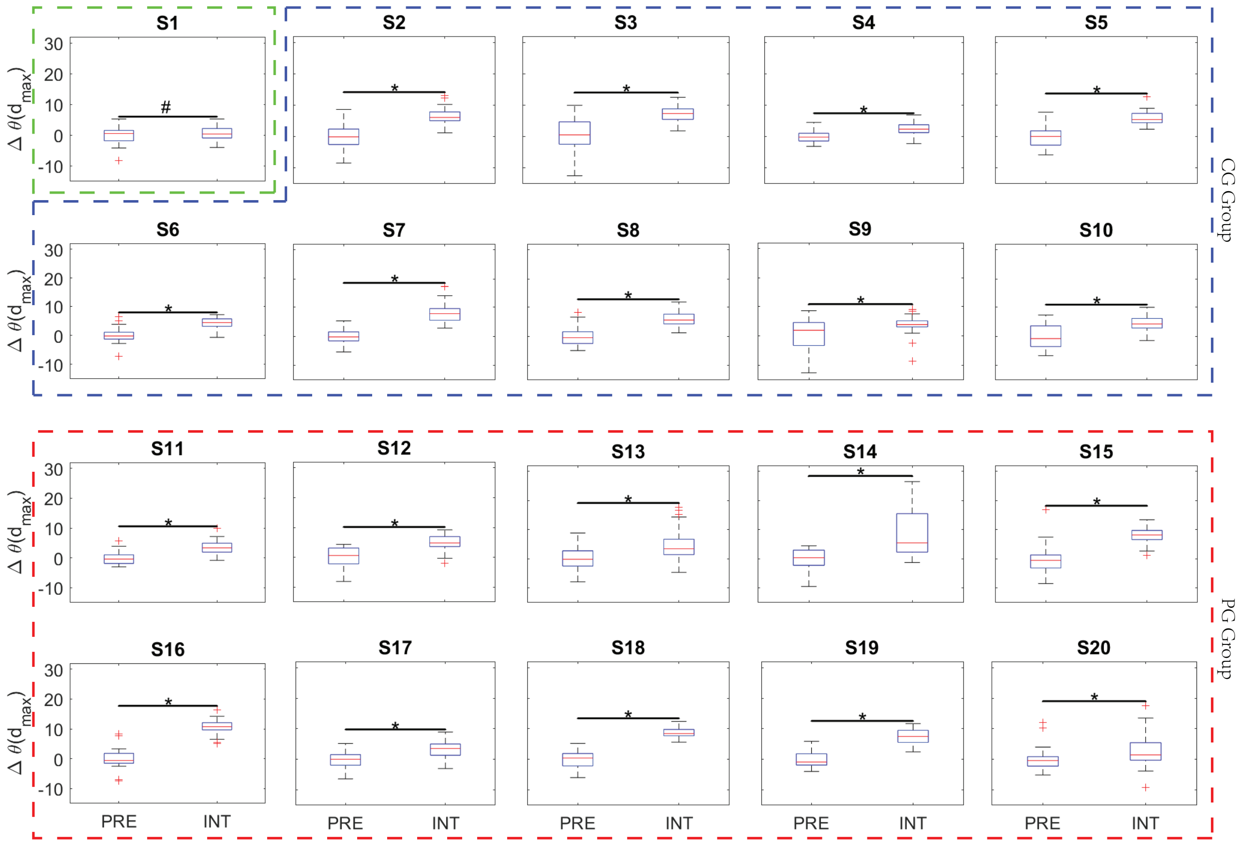

Fig. 3. The box plot shows individual intervention outcomes ($\Delta\theta(d_{max})$) in the comparative stage of INT phase (iterations 101 to 135) compared with the PRE phase. Subjects 1 to 10 were in the CG group and subjects 11 to 20 were in the PG group. The green, blue, and red boxes correspond to CG-NS, CG-S, and PG-S groups.

PG-S). Because substantial inter-subject variability in anthropometrics and baseline dynamics would likely obscure the relationship between swivel angle change and cost evolution, averaging energetic cost curves across subjects was avoided. Instead, the representative subject in each group was defined as the one whose adaptation magnitude, $\Delta\theta(d_{\max})$, was closest to the group mean. This yielded Subject 1 (CG-NS), Subject 6 (CG-S), and Subject 14 (PG-S). Their anthropometric parameters and adaptation outcomes are listed in Table 1, and the continuous cost-trend analysis focuses on these three representative subjects.

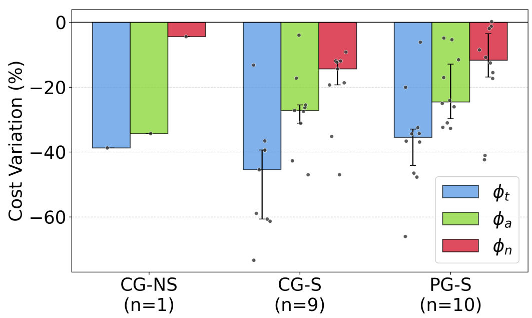

Fig. 4. The total (ϕ_t, blue), artificial (ϕ_a, green) and natural (ϕ_n, red) cost variation across the three experimental groups.

Table 1. Anthropometric parameters and outcomes of the representative subjects.

Group	Subj.	l_1 (m)	l_2 (m)	m_1 (kg)	m_2 (kg)	$\Delta\theta(d_{\max})$ (°)
CG-NS	1	0.35	0.33	3.0	2.8	-0.1
CG-S	6	0.36	0.29	3.5	3.2	4.4
PG-S	14	0.37	0.35	5.1	4.6	5.5

5. RESULTS

The relative cost variations for the CG-NS, CG-S, and PG-S groups are shown in Figure 4. The total cost variation (ϕ_t) is decomposed into the artificial force-field contribution (ϕ_a) and the natural dynamics contribution (ϕ_n). Across all three groups, the reduction in artificial cost was the main driver of the total energy saving. Specifically, ϕ_a contributed -34.27% of the total -38.68% for the CG-NS group, -27.20% of -45.45% for the CG-S group, and -24.53% of -35.47% for the PG-S group.

The relationship between estimated motor cost and average swivel angle change ($\Delta\bar{\theta}$) is shown in Figure 5 (top row). For all representative subjects, the total cost ($\mathcal{L}_t$, blue line) shows a steep negative gradient, decreasing by about 40% across the plotted range as swivel angle increases. The natural cost ($\mathcal{L}_n$, red line) decreases more gradually. This indicates that the change in total energy expenditure was dominated by the artificial cost component rather than by the limb's natural dynamics over the

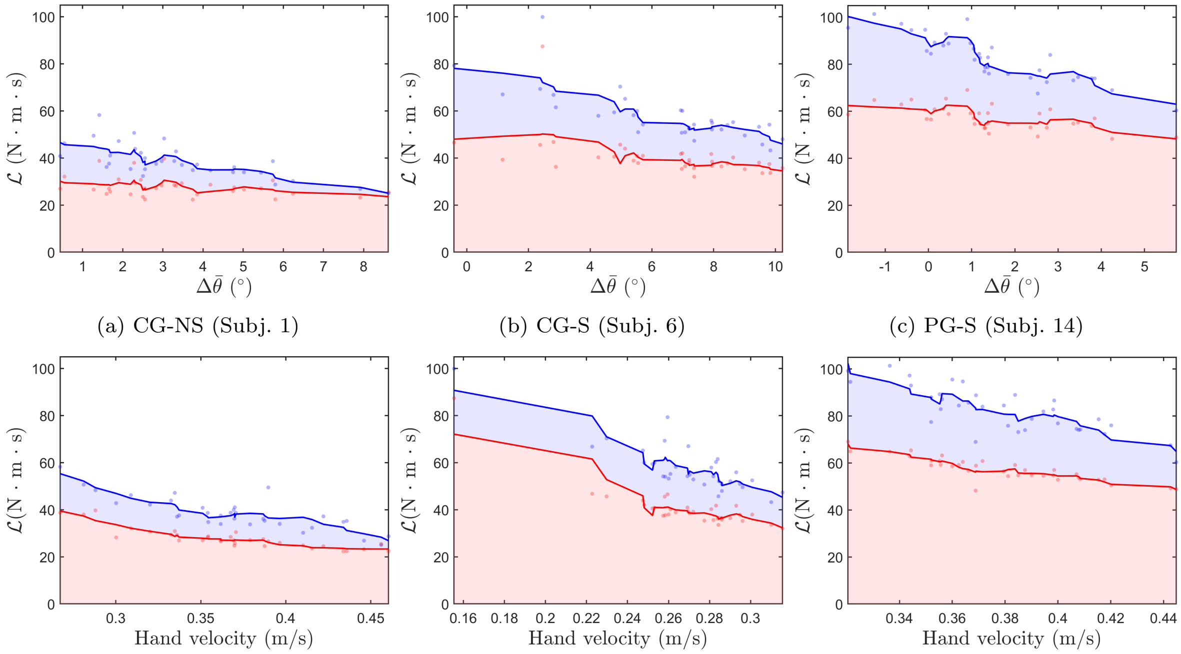

(a) CG-NS (Subj. 1) (b) CG-S (Subj. 6) (c) PG-S (Subj. 14)

(d) CG-NS (Subj. 1) (e) CG-S (Subj. 6) (f) PG-S (Subj. 14)

Fig. 5. Estimated motor cost for representative subjects as a function of swivel angle change ($\Delta\bar{\theta}$; top row) and hand velocity (bottom row). Blue lines indicate Total Cost ($\mathcal{L}_t$) and red lines indicate Natural Cost ($\mathcal{L}_n$).

swivel angle range. Notably, the same negative gradient is observed for Subject 1 (CG-NS, Figure 5a) and for the adapting subjects (Figure 5b, c). This indicates that a similar negative cost gradient was present in the non-adapting and adapting subjects, despite negligible behavioral change in the former ($\Delta\theta(d_{max}) \approx -0.1°$) relative to the latter (Subject 6, CG-S: $\Delta\theta(d_{max}) = 4.4°$; Subject 14, PG-S: $\Delta\theta(d_{max}) = 5.5°$).

The relationship between motor cost and hand velocity is shown in Figure 5 (bottom row). For all representative subjects, higher hand velocities were associated with lower natural and total motor costs, with reductions across the observed velocity range of approximately 39% and 43%, respectively. This pattern is consistent with the time-dependent nature of the TTI, for which higher velocities reduce the integration time.

6. DISCUSSION

6.1 Motor Cost Drives Motor Adaptation

This study investigated the physiological drivers of motor adaptation in ISC. Using the TTI to estimate energy expenditure, we found that the total motor cost, $\mathcal{L}_t$, decreased substantially with increasing swivel angle (Fig. 4). This reduction, corresponding to 30–40% of estimated total motor cost, provides a strong energetic incentive for the observed behavioral changes. Extending the theoretical cost compromise simulated in (Xu et al., 2021), this retrospective kinetic decomposition is consistent with synergy plasticity. By quantifying the proportion of energy savings attributable to the artificial component, we interpret synergies as stable solutions to a cost function that can be reshaped by external dynamics. Decomposing the total cost into natural and artificial components showed that adaptation was primarily driven by minimization of the robot-induced load. The artificial component (ϕ_a) dominated the total energy saving across all groups, confirming that the viscous force field created a steep energetic gradient in the redundant joint space. By penalizing low swivel angles, the robot made the baseline trajectory metabolically costly. The observed adaptation is consistent with participants exploiting a lower-cost region of the altered solution space. This shift toward a lower-cost region suggests that robotic interventions can reshape motor costs without explicit error feedback, in a manner consistent with motor-plasticity theories (Herzog et al., 2025).

For the single non-adapting participant (CG-NS, N = 1), the result should be interpreted as an individual case observation. Despite facing the same energetic gradient as the adapting groups, this participant did not explore it behaviorally. This suggests that energetic incentives alone are insufficient for adaptation. Implicit learning depends on motor variability to explore the solution space (Wu et al., 2014); if intrinsic variability is too low, or if the gradient is too shallow relative to sensory noise, the lower-cost solution may not be discovered. Future interventions may benefit from facilitating exploration, for example through dither signals or error augmentation, to guide participants out of local minima and toward a new synergy.

6.2 Coupling Between Hand Velocity and Motor Cost

The analysis also revealed a coupling between hand velocity and motor cost. The natural cost ($\mathcal{L}_n$) showed a shallow decline with increasing swivel angle, contrary to the expectation that lifting the elbow against gravity would increase effort. However, this should not be interpreted as evidence that larger swivel angles intrinsically reduce natural effort. Because TTI accumulates over time, both $\mathcal{L}_n$ and $\mathcal{L}_t$ are sensitive to movement duration. The decline in $\mathcal{L}_n$ with increasing swivel angle therefore likely reflects correlated variation in movement duration and hand velocity within the analyzed intervention trials, rather than a direct energetic benefit of swivel angle itself. This interpretation is consistent with Fig. 5, where higher hand velocities were associated with lower natural and total motor costs.

This within-condition trend does not imply that participants moved faster overall during adaptation. When comparing phases, participants reduced their average speed by 16–20% during the intervention relative to PRE (Xu et al., 2021). If the CNS were minimizing only total metabolic cost, movements should have become faster. Instead, the observed slowing suggests the influence of additional constraints, such as limiting peak force or maintaining stability. This trade-off is consistent with the viscous nature of ISC ($\mathbf{f}_{vis} \propto \dot{\mathbf{x}}$): moving faster reduces total TTI but increases instantaneous resistive force. The CNS therefore appears to prioritize limiting peak interaction forces and torque rates over minimizing total TTI. This interpretation is consistent with the "force-rate" hypothesis (Wong et al., 2025) and the "greedy optimization" framework (Emken et al., 2007).

These findings have practical implications for rehabilitation. If a therapeutic force field is too strong, patients may compensate by slowing down rather than by reshaping coordination. Future ISC designs should therefore balance gradient magnitude against perceptibility. Participants also rarely reached the full shaping goal of 10°, typically plateauing at 4.5–6°. This partial adaptation may reflect "motor slacking": once the resistive force falls below a perceptible threshold, the incentive for further adaptation declines, and the motor system settles on a tolerable rather than optimal solution. This suggests that implicit energy gradients must remain salient across the full adaptation range; one possible strategy is nonlinear gain scheduling for b_k to increase the penalty near the plateau.

Although TTI captures load-dependent metabolic cost, it does not account for muscle co-contraction. The observed slowing may therefore have been accompanied by increased joint stiffness, which should be examined in future studies using EMG. Overall, effective implicit shaping interventions must be strong enough to overcome habitual costs and prevent motor slacking, yet bounded enough to avoid compensatory slowing.

7. CONCLUSION

This study provides a quantitative analysis of the motor-cost mechanisms underlying Indirect Shaping Control (ISC). Using experimental kinematic data and a 4-DOF rigid-body model of the upper arm and forearm, we resolved the full 3D kinetics associated with swivel-angle changes and quantified motor cost via the Torque-Time Integral (TTI), decomposed into natural and robot-induced components. The results show that adaptation was primarily driven by reduction of the artificial viscous load, while the observed slowing of movement indicates a trade-off between cumulative energy and instantaneous interaction force. These findings provide a quantitative interpretation for designing implicit robotic interventions that reshape movement patterns without explicit error feedback.

REFERENCES

Emken, J., Benitez, R., Sideris, A., Bobrow, J., and David, R. (2007). Motor adaptation as a greedy optimization of error and effort. *J. Neurophysiol.*, 97(6), 3997–4006.

Flash, T. and Hogan, N. (1985). The coordination of arm movements: an experimentally confirmed mathematical model. *J. Neurosci.*, 5(7), 1688–1703.

Fong, J., Crocher, V., Tan, Y., and Oetomo, D. (2019). Indirect robotic movement shaping through motor cost influence. In *International Conference on Rehabilitation Robotics (ICORR)*, 977–982. Toronto, Canada.

Fong, J., Crocher, V., Tan, Y., Oetomo, D., and Mareels, I. (2017). Emu: A transparent 3d robotic manipulandum for upper-limb rehabilitation. In *International Conference on Rehabilitation Robotics (ICORR)*, 771–776.

Herzog, M., Berger, D., Russo, M., d'Avella, A., and Stein, T. (2025). Changes in muscle synergy structure and activation patterns underlie force field adaptation, retention, and generalization. *J. Neurophysiol.*, 134(6), 2047–2069.

Kang, T., He, J., and Tillery, S. (2005). Determining natural arm configuration along a reaching trajectory. *Exp. Brain Res.*, 167(3), 352–361.

Levin, M., Kleim, J., and Wolf, S. (2009). What do motor recovery and compensation mean in patients following stroke? *Neurorehabil. Neural Repair*, 23(4), 313–319.

McMorland, A., Runnalls, K., and Byblow, W. (2015). A neuroanatomical framework for upper limb synergies after stroke. *Front. Hum. Neurosci.*, 9, 82.

Plagenhoef, S., Evans, F.G., and Abdelnour, T. (1983). Anatomical data for analyzing human motion. *Res. Q. Exerc. Sport.*, 54(2), 169–178.

Reinkensmeyer, D., Akoner, O., Ferris, D., and Gordon, K. (2009). Slacking by the human motor system: computational models and implications for robotic orthoses. In *International Conference of the IEEE Engineering in Medicine and Biology Society*, 2129–2132.

Rozand, V., Cattagni, T., Theurel, J., Martin, A., and Lepers, R. (2015). Neuromuscular fatigue following isometric contractions with similar torque time integral. *Int. J. Sports Med.*, 36(01), 35–40.

Russ, D., Elliott, M., Vandenborne, K., Walter, G., and Binder-Macleod, S. (2002). Metabolic costs of isometric force generation and maintenance of human skeletal muscle. *Am. J. Physiol. Endocrinol. Metab.*, 282(2), E448–E457.

Todorov, E. and Jordan, M. (2002). Optimal feedback control as a theory of motor coordination. *Nat. Neurosci.*, 5(11), 1226–1235.

Uno, Y., Kawato, M., and Suzuki, R. (1989). Formation and control of optimal trajectory in human multijoint arm movement. *Biol. Cybern.*, 61(2), 89–101.

Wong, J., Herspiegel, W., and Kuo, A. (2025). Energy and time trade-offs explain everyday human reaching movements. *bioRxiv*.

Wu, H., Miyamoto, Y., Castro, L., Ölveczky, B., and Smith, M. (2014). Temporal structure of motor variability is dynamically regulated and predicts motor learning ability. *Nat. Neurosci.*, 17(2), 312–321.

Xu, Y., Crocher, V., Fong, J., Tan, Y., and Oetomo, D. (2021). Inducing human motor adaptation without explicit error feedback: A motor cost approach. *IEEE Trans. Neural Syst. Rehabil. Eng.*, 29, 1403–1412.